NUMERICAL CHARACTERIZATION OF THE DISCHARGE COEFFICIENT IN CRITICAL NOZZLES

Presenter:
A. N. Johnson
National Institute of Standards and Technology
Gaithersburg, Maryland 20899
Fluid Mechanics Bldg., Rm 105
Phone: (301)-975-5954
Fax: (301) 258-9201

Paper Authors:
A. N. Johnson,* P. I. Espina,* G. E. Mattingly,† J. D. Wright*
and
C. L. Merkle‡
University of Tennessee Space Institute
Tullahoma, Tennessee 37388

ABSTRACT

The discharge coefficient in critical nozzles flowing N_2, Ar, CO_2, and H_2 in the Reynolds number range (2 000 to 22 000) is studied computationally to assess the capability of Computational Fluid Dynamics (CFD) in assisting experimental calibration. A parametric study is conducted to investigate the effects of the wall thermal boundary condition and gas species on the calibration process. Comparisons between numerical and experimental data are found to be in good agreement. However, similar to existing analytical models, the computational model has difficulty characterizing the discharge coefficient for CO_2. Based on these results, it is concluded that with continued research CFD may have the potential to aid in the calibration of critical nozzles by providing detailed flow field characteristics for operating conditions and nozzle geometries not conducive to experiment.

NOMENCLATURE

A	area
C^*	critical flow factor, $= \sqrt{\gamma}\,(\frac{\gamma+1}{2})^{\frac{(\gamma+1)}{2(1-\gamma)}}$

*Mechanical Engineer, Fluid Flow Group, Bldg. 230, Rm. 105.
†Leader, Fluid Flow Group, Bldg. 230, Rm. 105.
‡H.H. Arnold Chair

C_d	discharge coefficient
c_P	specific heat at constant pressure, $= (\frac{\gamma R}{\gamma - 1})$
d	nozzle throat diameter, = 0.5935 mm
k	thermal conductivity
M	Mach number
$\dot{m}$	mass flow rate
MW	molecular weight
n	normal direction
P	pressure
Pr	Prandtl number, $= \frac{\mu c_P}{k}$
R	nozzle throat radius, = d/2
Re	Reynolds number based on diameter
R_{gas}	gas constant, $= R_u/MW$
R_u	universal gas constant
R_c	radius of curvature at nozzle throat
r	radius or radial coordinate
T	temperature
x	axial coordinate
U_r	experimental expanded uncertainty

α	inviscid discharge coefficient
β	magnitude of the slope of the calibration curve
γ	specific heat ratio
δ_{th}	thermal boundary layer thickness
θ	half angle of nozzle divergent section, = 0.05236 radians, (3°)
μ	molecular viscosity
ρ	density

Subscripts

amb	ambient conditions outside nozzle configuration
adia	adiabatic wall condition
hot	constant wall temperature equal to ambient temperature
ideal	based on one dimensional inviscid analysis
o	stagnation condition
real	based on experimental data
wall	conditions at the wall

Superscripts

*	conditions at throat assuming one-dimensional inviscid flow

INTRODUCTION

Critical nozzles offer a reliable and accurate method of measuring gas mass flow rate and play an important role in many industrial processes. These devices are used as gas flow meters, calibration standards for other gas flow meters, and flow control/limiting devices. In the past, high fabrication cost restricted industrial use of critical nozzles, but advances in computer controlled machining has reduced manufacturing cost allowing increased usage for industrial applications.

One dimensional inviscid flow theory can be used to predict the metrological performance of sonic nozzles. Using this approach, it can be shown that the "ideal" mass flow rate through a nozzle is governed by the following relationship[1]

$$\dot{m}_{\text{ideal}} = \frac{P_o A^* C^*}{\sqrt{R_{\text{gas}}\, T_o}} \tag{1}$$

where P_o is the stagnation pressure, T_o is the stagnation temperature, C^* is the critical flow factor (a function of the specific heat ratio, γ), A^* is the nozzle throat area, and R_{gas} is the gas constant for a given specie. The analytical model assumes that the flow through the nozzle is at choked conditions (*i.e.*, $M^* = 1$), and it gives a convenient expression for gas mass flow rate, but it provides only limited accuracy (expanded uncertainty, $U_r \approx 4\,\%$ of reading).

If more accuracy is required by the application, calibration of the critical nozzle is recommended. Calibration supplements one dimensional inviscid flow theory by including a discharge coefficient in Equation (1). The discharge coefficient is defined as

$$C_d \equiv \frac{\dot{m}_{\text{real}}}{\dot{m}_{\text{ideal}}} \tag{2}$$

where $\dot{m}_{\text{real}}$ is the mass flow rate measured experimentally.

For a given nozzle geometry, the discharge coefficient changes as a function of the flow rate passing through it. Traditionally, this functionality has been expressed in terms of a reference Reynolds number defined as[2]

$$Re^*_{\text{real}} = \frac{4\,\dot{m}_{\text{real}}}{\pi\, d\, \mu_0} \tag{3}$$

where d is the nozzle throat diameter and μ_0 is the molecular viscosity at stagnation conditions. This calibration procedure, although expensive, enables high accuracy gas mass flow measurements ($0.1\,\% \leq U_r \leq 0.3\,\%$) over a wide range of operating conditions.

In an effort to eliminate the need for calibration, previous research has focused on the development of more complex models capable of predicting nozzle performance at improved

levels of accuracy. Several researchers[3-6] have developed analytical models that characterize the discharge coefficient over a wide range of operating conditions as a function of various physical parameters. In particular corrections for multi-dimensional effects and for viscous effects have been developed. While these models do not yield the same level of accuracy provided by calibration, they offer considerable improvement over the results of the one-dimensional inviscid flow model.

In 1962, Hall[3] implemented a power series solution to the axisymmetric compressible potential flow equation to determine an analytical expression characterizing the effect of an axisymmetric velocity profile on the discharge coefficient. His approach improved upon one dimensional inviscid theory by incorporating multi-dimensional effects into the analysis. Following this research, Geropp[4] and Tang[5] independently used laminar boundary layer flow theory to develop expressions relating the discharge coefficient to Re^*_{ideal}, γ, and nozzle geometry. Here Re^*_{ideal} is an ideal version of the reference Reynolds number. Their results provided insight into how viscous effects impact the discharge coefficient. However, both sets of results incorporated assumptions that limit their general application. In addition, Geropp's and Tang's methods do not include multi-dimensional effects that are inherent to the core flow inside the nozzle, and thus the models cannot completely characterize the discharge coefficient by themselves.

Ishibashi and Takamoto[6] combined and extended the previous analytical models of Hall[3] and Geropp[4] to obtain a more suitable analytical expression. While their model also expresses the discharge coefficient as a function of Re^*_{ideal}, γ, and nozzle geometry, it incorporates both multi-dimensional and viscous effects. When compared with experimental results, the analytical expression of Ishibashi and Takamoto shows excellent agreement for a large number of gas species ($U_r \leq 0.5\,\%$), although its performance is poor for selected gases (*e.g.*, $U_r \approx 2.5\,\%$ for CO_2).

In the present investigation we assess the effectivness of using complete numerical solutions of the compressible Navier-Stokes equations to predict the experimentally observed physical behavior of flows in critical nozzles. The goal is to ascertain the level of agreement that can be obtained between numerical solutions and the experimental data, as well as the differences between the numerical predictions and the previously cited analytical models. The methodology is tested for four different gas species, (*i.e.*, Ar, N_2, CO_2, and H_2), and its ability to accurately characterize the discharge coefficient is assessed by direct comparison with experimental data.[7]

NUMERICAL METHOD

Governing Equations

The axisymmetric, steady, compressible flow through a critical nozzle is governed by the Navier-Stokes equations. In this work, the fluid is assumed to be a perfect gas having a constant specific heat, (*i.e.*, $c_P = constant$), and exhibiting a Newtonian stress-strain

behavior. The thermal conductivity and the molecular viscosity are related to temperature by the Sutherland viscosity law.[8] The effects of turbulence are not considered herein given that the Reynolds numbers range (2 000 to 22 000) is much lower than the experimentally viewed transition Reynolds number for critical nozzles (10^6).[9]

Numerical Algorithm

The numerical algorithm employs the strong conservative form of the Navier Stokes equation. Spatial discretization is achieved using up-winded, third-order finite differences, while time advancement is obtained using one-sided, first-order finite differences. The algorithm retains the time derivatives in the governing equations, utilizing a time marching procedure to advance the solution to steady state. Alternating-direction implicit factorization is implemented, employing both inviscid and viscous pre-conditioning[10–12] for convergence enhancement. Explicit fourth-order artificial dissipation is added to damp higher modes of transient errors, and the resulting block tridiagonal matrices are inverted using a block version of the Thomas algorithm at each time step.

Computational Domain and Boundary Conditions

The geometry of the critical nozzle studied in this investigation follows ISO[13] standards and is shown schematically in Figure 1. The contour of the axisymmetric converging-diverging nozzle has a converging section consisting of a circular arc that passes through the throat to a point of tangency at which the shape becomes conical. The grid for this geometry consisted of 201 grid points in the axial direction and 101 grid points in the radial direction. The grid cells in the radial direction were concentrated near the wall in order to resolve the high gradients present in the boundary layer region.

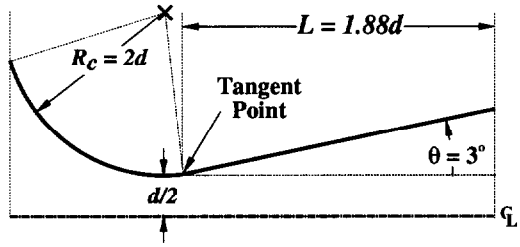

Figure 1. Schematic of critical nozzle geometry studied.

Figure 2 shows the orientation of a critical nozzle in a pipeline. This investigation neglects the pipeline geometry upstream of the nozzle geometry, modeling the nozzle region as depicted by the grey shaded area in Figure 2 (labeled computational domain). At the nozzle inlet T_0, P_0, and the flow angle are fixed. Symmetry conditions are applied along the centerline. The computations are taken to be fully supersonic so explicit extrapolation of the inner characteristic variables is applied at the exit plane in accordance with the method of characteristics. No-slip boundary conditions are applied at the nozzle wall with an appropriate thermal boundary condition (adiabatic or specified wall temperature as indicated on the figure).

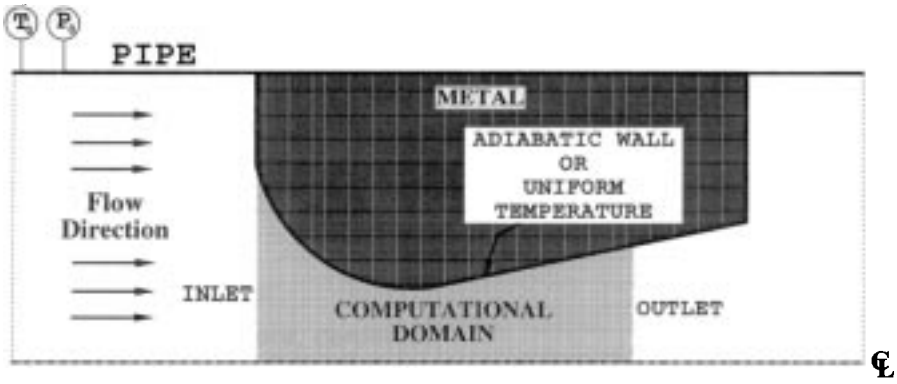

Figure 2. Schematic of critical nozzle geometry in pipeline: Computational Domain shaded grey ($P_0 \simeq$ (0.25 atm) 25 332.5 Pa $\rightarrow$ (2.0 atm) 202 660 Pa, $T_0 = 298.15$ K).

RESULTS

Dimensional analysis of the governing flow equations[3-6] shows that the dimensionless parameters influencing the discharge coefficient, C_d, are: Re^*_{ideal}, γ, Pr, and T_{wall}/T_0.[†] A simple way to study the functionality of C_d on Re^*_{ideal} is to vary the upstream stagnation conditions (*i.e.*, P_0 and T_0). The functionality of C_d on γ can be studied by computing results for various gas species. However, gas species affect more than one dimensionless parameter and thus, changes in gas specie will also result in minor changes of the Re^*_{ideal} and Pr as a result of the functionality of these parameters on fluid properties. Both the effects of Re^*_{ideal} and γ are considered by the previously mentioned analytical models,[3-6] while the effects of Pr and wall thermal boundary condition – T_{wall}/T_0, are not. In this investigation we seek to analyze the influence of the four previously mentioned dimensionless parameters on C_d using CFD results in combination with a sensitivity analysis.

In the first part of this investigation we considered the variation of C_d with Re^*_{ideal} for N_2, Ar, CO_2, and H_2. The numerical computations were validated by comparing the predictions with the experimental results of Nakao *et al.*[7] for Re^*_{ideal} ranging from 2 000 to 22 000. Although the predictions for N_2, Ar, and H_2 were found to be in good agreement with the experimental measurements, the CO_2 predictions were consistently less accurate. Similar results have also been reported when using the composite analytical model[6] to predict the experimental data. In what follows, this discrepancy will be addressed in more detail and computational results will be used to assess the assumption of $Pr = 1$ and the adiabatic wall condition used in the composite analytical model.[6] The physical mechanisms affected by these assumptions will be outlined and the overall impact of the four dimensionless parameters on C_d will be discussed.

[†]The geometry of the nozzle wall plays an important role in the determination of the discharge coefficient characteristics of a given nozzle.

Comparison between Analytical, Experimental, and Numerical Results.

We begin by comparing the numerically predicted calibration curves with the analytical[6] and experimental[7] counterparts. Four sets of C_d *vs.* Re^*_{ideal} (*i.e.*, calibration curves) are given in Figure 3 along with corresponding experimental[7] and analytical[6] results for the given gases. The abscissa of these curves is expressed in terms of $1/(Re^*_{\text{ideal}})^{1/2}$ which has the effect of linearizing the results, as predicted by analytical model.[6] In all curves, the ×'s label the numerical data, the dashed line (- - -) represents the analytical data,[6] and the •'s label the experimental results.[7] The size of the •'s represents the uncertainty of the experimental measurements,[7] which was nearly equal nearly equal in all the cases.

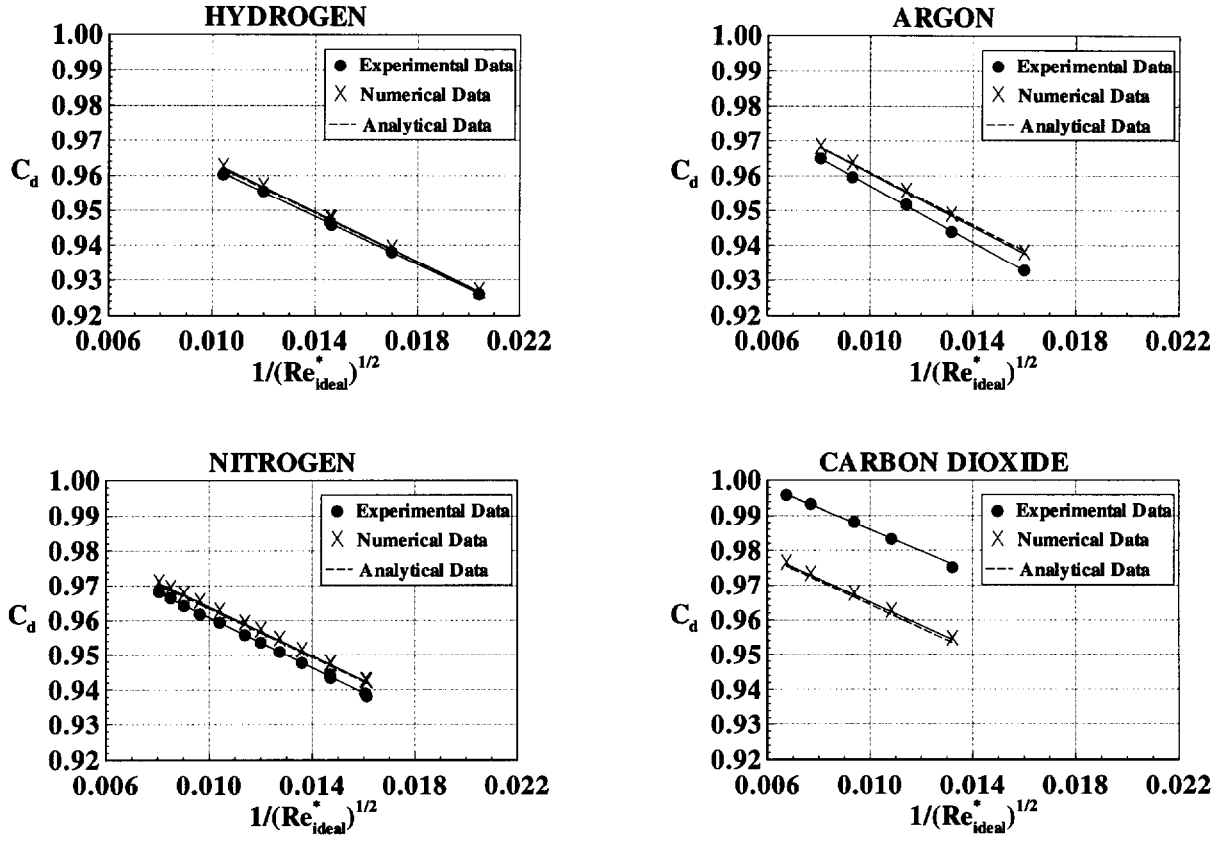

Figure 3. Comparison between analytical,[6] numerical and experimental[7] sonic nozzle discharge coefficients for four gas species. (Adiabatic nozzle wall assumed in computations). $\gamma_{N_2} = 1.4$, $\gamma_{Ar} = 1.67$, $\gamma_{H_2} = 1.409$, $\gamma_{CO_2} = 1.3$.

From Figure 3, it can be observed that the numerical results are in good agreement with the analytical model of Ishibashi and Takamoto.[6] In particular, both the numerical and analytical results[6] share agreement in both slope and intercept of the calibration curves. The largest difference between the two sets of data is less than 0.14 % in magnitude. This seems to suggest that the composite analytical model of Ishibashi and Takamoto adequately characterizes the viscous and multi-dimensional effects present in ISO[13] nozzles.

When compared with the experimental data,[7] the numerical results exhibit the same trends (*i.e.*, their slopes are almost identical). However, throughout the range of Re^*_{ideal} the two sets of data differ by a nearly constant offset. For H_2, N_2, and Ar, the computational results predicted higher values of C_d than the experiments. The magnitude of the offset between experimental[7] and computational results differed for each gas species, with the maximum difference between the two sets of results being: +0.20 % H_2, +0.43 % N_2, +0.49 % Ar. In contrast, the CO_2 results underpredict the experimental measurements,[7] and the magnitude of this error (-2.15 %) is nearly an order of magnitude larger than the errors seen for the other gases.

The results for H_2, N_2, and Ar appear to follow trends that can be physically justified. The assumption of uniform irrotational inflow (*i.e.*, negligible boundary layer thickness at nozzle inlet) used as the upstream boundary condition for the numerical simulations matches that used in the composite theory[6] and gives almost identical results. Further, the predicted C_d's exceed the measured[7] ones suggesting that the computational model underpredicts the boundary layer thickness along the nozzle wall. It is hoped that extending the computational domain to incorporate the effects of the upstream piping geometry will provide the proper (non-zero) nozzle inlet boundary layer thickness. Accordingly, the thicker boundary layer could reduce the predicted level of C_d bringing the numerical results into closer agreement with the experimental data.[7] In addition, possible flow separation in the vicinity of the nozzle inlet and cross stream variations in stagnation pressure could be simulated.

The predictions for CO_2 gas, however, are already too low and incorporating these "real" installation effects is expected to increase their discrepancy from the experimental data even more. The reasons for this unique behavior of CO_2 are unclear, but several possible effects have been investigated as it will be shown in the following sections.

Issues Involved in CO_2 Measurements/Predictions.

As indicated above (see Figure 3), both the composite analytical model[6] and the CFD predictions accurately characterize the experimental results for three (H_2, N_2, and Ar) of the gases. The CO_2 predictions, however, are underpredicted by more than 2 % by both the computations and the composite model.[6] Furthermore, improving the upstream conditions will almost certainly increase this error. This unexpected inability of the composite model[6] and the CFD analysis to predict the observed CO_2 performance indicates there may be something unique about this gas specie. Accordingly, several sensitivity levels were assessed to ascertain if their impact significantly affected the computed C_d for CO_2. First, the effects of the wall thermal boundary condition were considered. Second, an assessment of potential non-equilibrium effects of the flowing CO_2 was made. Third, deviations from ideal gas behavior were assessed, and finally, the experimental measurements for CO_2 were replicated in our laboratory in the unlikely event that there was some bias in the experimental measurements.[7] All these checks, however, were to no avail, and the discrepancy persists. We briefly summarize the results of each one below.

The wall temperature in critical nozzles must for physical reasons lie between the temperature predicted by the adiabatic assumption and the ambient temperature outside the nozzle. Therefore, the most significant effect that the wall thermal boundary condition could have on C_d can be investigated by replacing the adiabatic wall condition by a constant wall temperature equal to the ambient temperature (T_{amb} = 298.15 K). The percent change in C_d resulting from testing both limiting conditions gives an indication to the degree of sensitivity of C_d to wall thermal boundary conditions. When $T_{wall} = T_{amb}$ the results showed that C_d decreased which made the observed discrepancy for CO_2 between the computational and experimental results even larger, and as a result the inclusion of this effect is not likely to be at fault for the observed discrepancy.

Next we assessed the possible physical mechanisms unique to CO_2 that might explain the observed discrepancy. Axial gradients in thermodynamic properties, within the nozzle convergent flow, raised the possibility that non-equilibrium (relaxation) effects might be present. The vibrational relaxation time (*i.e.*, time necessary for redistribution of internal energy to vibrational degrees of freedom when a fluid particle is subjected to a change in thermodynamic environment) for CO_2 is on the order of 10^{-5} s at T = 300 K and P = (1 atm) 101 330 Pa. Due to the small spatial size of the critical nozzle studied in this paper (*i.e.*, d = 0.5935 mm) the vibrational relaxation time (10^{-5} s) is on the same order as the time it takes a fluid particle to travel from the nozzle inlet to the throat (10^{-5} s). Therefore vibrational non-equilibrium may contribute to the discrepancy observed in the CO_2 results and we are continuing research to explore this possibility.

Next, we focused on the thermodynamic deviations of CO_2 properties from ideal gas behavior. Over the range of pressures and temperatures experienced by the CO_2 flow through the nozzle ($P \simeq$ (0.25 atm) 25 332.5 Pa $\rightarrow$ (2.0 atm) 202 660 Pa, $T \simeq$ 250 K $\rightarrow$ 300 K), the compressibility factor for CO_2 varies by only 1.0 %, a value that does not appear to have significant effect on the present results. Nevertheless a more in-depth investigation is necessary to determine the magnitude and sign of changes caused by real gas effects.

Finally, and as a last resort, the experimental measurements[7] with CO_2 were replicated in the NIST calibration laboratory to assure the discrepancy was not caused by experimental bias. The NIST results confirmed the data of Nakao *et al.* as expected. In summary, few plausible reasons for the differences between CO_2 and the other gases exist, and the most obvious ones have been investigated. Unfortunately the present analysis is inconclusive to determine what causes the unique behavior for CO_2. The difficulty with CO_2 would, however, appear to be of significance to the metering community, and requires additional study both experimentally and analytically. In the remaining sections we address primarily the results for the other three gases.

Physical Interpretation of the Calibration Curve

As demonstrated by Nakoa *et al.*[7], a convenient way to report nozzle calibration data is via C_d *vs.* $1/(Re^*_{ideal})^{1/2}$ curves. Although this linear behavior only holds true for nozzle flows

with $Re^*_{\text{ideal}} < 10^6$ (*i.e.*, laminar flow, see Ref. 9), the expression of the data in this fashion enables the representation of the nozzle behavior using a two-parameter model

$$C_d = \alpha - \beta/\sqrt{Re^*_{\text{ideal}}} \tag{4}$$

In the above expression, α is the y-intercept of the calibration curve (see Figure 3) and β is the magnitude of its slope. Physically, α represents the discharge coefficient for an inviscid flow (*i.e.*, $Re^*_{\text{ideal}} \to \infty$) and it is a measure of the influence of multi-dimensional phenomena on the discharge coefficient. The parameter β is proportional to the reduction in C_d due to viscous effects (*i.e.*, the boundary layer thickness at the nozzle throat).

Table 1 shows the variation of α and β as a function of γ for the four gas species considered. Similar to the trends observed for C_d, the numerical results for N_2, H_2, and Ar overpredict α while the results for CO_2 are grossly underpredicted. The numerical results (see Table 1) indicate that the magnitude of slopes (β) of the calibration curves decreases as γ decreases. While this trend is true for the limited number of gases considered here, when additional gases from the experimental data[7] are considered (*e.g.*, SF_6, C_2H_2, C_2H_6, CH_4) it is found that CO_2 is an outlier of this trend.

Gas	γ	α_{exp}	α_{num}	$\alpha_{\%diff}$	β_{exp}	β_{num}	$\beta_{\%diff}$
CO_2	1.300	1.0168	0.9989	-1.76	3.077	3.370	+9.52
N_2	1.400	0.9970	0.9992	+0.22	3.618	3.531	-2.40
H_2	1.409	0.9967	0.9995	+0.28	3.458	3.568	+3.18
Ar	1.667	0.9976	0.9990	+0.14	4.053	3.830	-5.50

Table 1. Functionality of two-parameter calibration curves on gas specie.

The numerical results qualitatively agree with the experimental data, making it reasonable to use the computational model to disseminate trends resulting from systematically varying the governing dimensionless parameters (*i.e.*, $Pr, \gamma, T_{wall}/T_0$). The remainder of this paper will assess the importance of these parameters in critical nozzle calibration by determining their influence on C_d.

Effect of Prandtl Number

The analytical methods[3–6] described in the introduction make the fundamental assumption of equality between the magnitudes of molecular- and thermal-diffusivity (*i.e.*, $Pr = 1$). Although most gases used in critical nozzle applications have $Pr \approx 0.7$ (see Ref. 14), the $Pr = 1$ assumption appears to be warranted based on the close agreement between numerical and analytical results[6] shown earlier in Figure 3. In what follows, a sensitivity analysis is performed to quantify the effect between $Pr = 1.0$ (*i.e.*, assumed in analytical models) and $Pr = 0.7$ (*i.e.*, actual value for most gases) on C_d. For this comparison the nozzle wall is taken to be adiabatic. The results here presented are for N_2, but their implications apply to other gas species.

Under the assumption of ideal gas and $Pr = 1$, the rate of work done by viscous forces is balanced by the conduction heat losses within the thermal boundary layer. When $Pr < 1$, the ability of a thermal boundary layer to effectively diffuse heat generated by viscous dissipation is enhanced. Consequently, radial conduction distributes heat over a larger affected volume (*i.e.*, a thicker thermal boundary layer) leading to lower temperatures near the wall and slightly higher temperatures near the free stream. Figure 4 compares the normalized throat radial temperature distributions, T/T^*, for $Pr = 1$ and $Pr = 0.7$, illustrating this effect. The figure only illustrates the behavior close to the wall given that outside of the thermal boundary layer the influence of Pr vanishes.

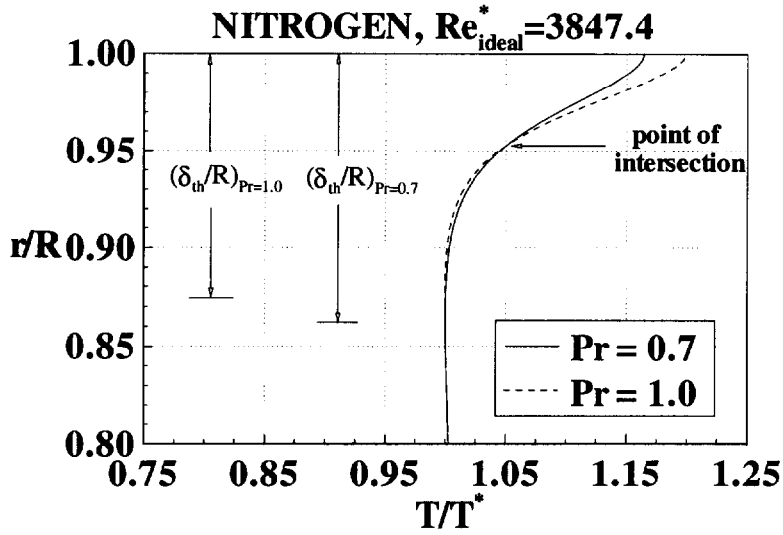

Figure 4. Effect of Prandtl number on heat dissipation near the wall (nozzle throat radial temperature profiles). --- $Pr = 0.7$; —— $Pr = 1.0$. [Included in the figure are the thermal boundary layer thicknesses: $(\delta_{\text{th}}/\text{R})|_{\text{Pr}=0.7} = 0.138$; $(\delta_{\text{th}}/\text{R})|_{\text{Pr}=1.0} = 0.126$).]

As shown in Figure 4 the temperature distribution within the thermal boundary layer only changes slightly when Pr is reduced from $Pr = 1$ to $Pr = 0.7$. Specifically $T_{Pr=0.7}$ is lower than $T_{Pr=1.0}$ near the wall ($\approx 2.8\,\%$ lower) while the trend reverses further away from the wall ($0.862 \geq r/R \geq 0.952$) where $T_{Pr=1.0}$ is $\approx 0.33\,\%$ higher. The changes in pressure and velocity due to changes in Pr are small, and therefore the density varies inversly to temperature, increasing near the wall ($+2.77\,\%$) and decreasing slightly ($-0.49\,\%$) near the free stream. The difference in the radial density profile when $Pr < 1$ is the predominant factor controlling the difference in the streamwise throat mass flux distribution. The difference in the mass flux profiles between $Pr = 0.7$ and $Pr = 1.0$ is shown in Figure 5. (Note that the abscissa has been chosen so that integrating across the throat cross section yields the difference in C_d between the two Pr). This figure shows that the increase of mass flux near the wall more than compensates for the deficit of mass flux near the free stream, and thus, the overall average mass flux increases as Pr decreases from unity.

The mass flux profiles of Figure 5 were integrated across the throat cross section to determine C_d, and the functionality of C_d with Pr is shown in Figure 6. In addition to $Pr = 0.7$ and

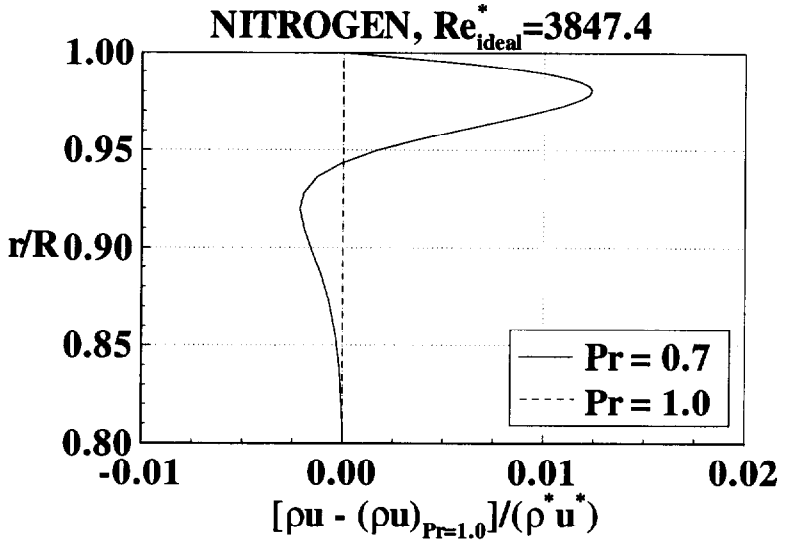

Figure 5. Difference in streamwise mass flux for $Pr = 0.7$ and $Pr = 1.0$ (Adiabatic Wall Condition)

$Pr = 1.0$, we considered $Pr = 0.1$ and $Pr = 10.0$ (although not physically attainable for most gases) to clearly illustrate the effect of Pr on C_d. The figure shows that C_d increases in a non-linear manner as Pr is decreased; however the difference between C_d for the value of $Pr = 1.0$ (used in analytic models) and $Pr = 0.7$ (value for most gases) is only 0.06 %. As a result, we can conclude that the assumption of $Pr = 1$ made in the analytical models[3-6] does not significantly degrade their performance.

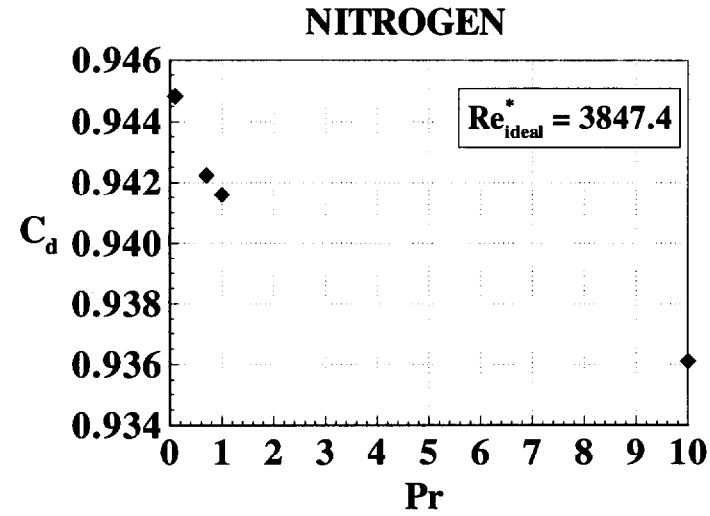

Figure 6. C_d variation versus Pr (Adiabatic Wall Condition)

Effect of Wall Thermal Boundary Condition

The adiabatic wall condition ($\partial T/\partial n = 0$) is used in the composite analytical model of Ishibashi and Takamoto,[6] as well as in the present computational model. For critical nozzles

under normal calibration conditions ($T_{amb} = T_0$, $Re^*_{ideal} >> 1$, and $Pr \approx 0.7$) the adiabatic wall assumption seems to be justified as shown previously by the close agreement between analytical[6] and numerical results in Figure 3. However, the assumption is not strictly valid; under normal calibration conditions the ambient temperature is larger than the adiabatic wall temperature (*i.e.*, the wall temperature profile for an insulated wall) and heat flows from the environment into the fluid. In this section we determine the sensitivity of the discharge coefficient to wall thermal boundary conditions by comparing C_d predictions for an adiabatic wall condition with predictions for a "hot" wall condition, $T_{wall} = T_{amb}$ (298.15 K).

Physically, the hot wall condition ($T_{wall} = T_{amb}$) represents the maximum attainable wall temperature (under normal calibration conditions), and thus our investigation will determine the maximum possible influence of heat transfer on C_d. For the hot wall condition the effect of heat transfer is predominately confined to a thin region near the wall denoted as the thermal boundary layer. Increased temperatures in this region decrease both the density, and to a lesser extent, the flow velocity thus resulting in a lower mass flux. Figure 7 shows the difference in throat mass flux profile within the thermal boundary layer between the adiabatic wall condition and the hot wall condition for a typical flow. In the figure we can see that $\Delta C_d > 0$ (*i.e.*, $C_{d,adia} > C_{d,hot}$) due to increased mass flow throughout the thermal boundary layer for the adiabatic wall condition.

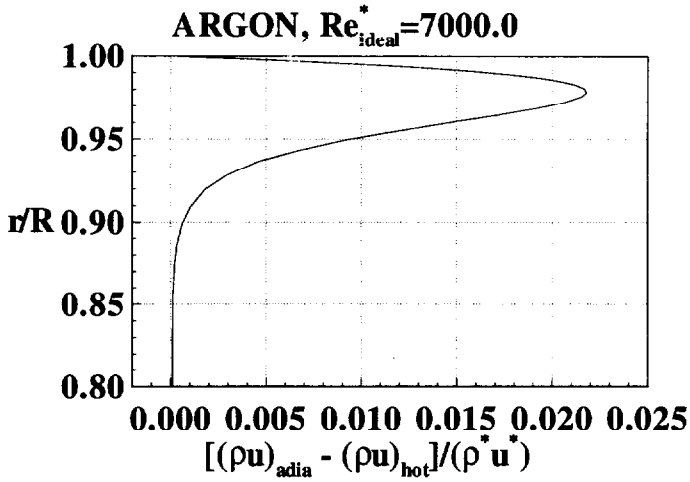

Figure 7. Difference of mass flux between an adiabatic wall and a hot wall at the nozzle throat for $Re^*_{ideal} = 7\,000$.

The sensitivity of the wall thermal boundary condition depends on both γ and Re^*_{ideal}. Figure 8 shows the numerical results for the change in C_d between an adiabatic wall and a hot wall for H_2, N_2, CO_2, and Ar. The effect of the wall thermal boundary condition is seen to be greatest at the lowest Re^*_{ideal} for all the gas species. At larger Re^*_{ideal}, forced convection heat transfer from the nozzle wall is enhanced, thus shrinking the thermal boundary layer and decreasing the effect of heat transfer. In the limit $Re^*_{ideal} \to \infty$ the difference in C_d becomes negligible ($\Delta C_d \to 0$) which indicates that C_d has little sensitivity to the wall thermal boundary condition at large Re^*_{ideal}.

The sensitivity of C_d to wall thermal boundary condition increases for gas species with larger γ. The effect that gas species have on the wall thermal boundary condition is also shown in Figure 8. Gases with larger γ are more significantly affected by the wall thermal boundary condition since larger γ's result in lower free stream throat temperatures, which in turn, cause the temperature difference responsible for heat transfer to increase. Increased heat transfer leads to decreased mass flux throughout the thermal boundary layer, and therefore, gases with larger γ are more sensitive to the wall thermal boundary condition than gases with lower γ.

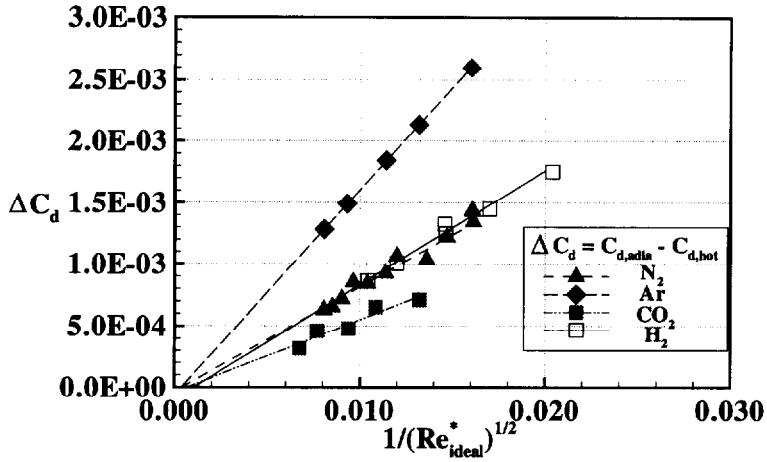

Figure 8. Change in Numerical Discharge Coefficient versus Throat Reynolds Number for H_2, Ar, N_2, and CO_2 for an adiabatic wall and hot wall.

Conclusions

CFD was utilized to characterize the discharge coefficient for N_2, Ar, H_2, and CO_2 in an ISO[13] critical nozzle for a Re^*_{ideal} range from 2 000 to 22 000. For N_2, Ar, and H_2 numerical results matched trends exhibited by experimental data, and the accuracy of the numerical solutions was within acceptable limits ($U_r \leq 0.5\,\%$) over the range of computed Re^*_{ideal}. It is expected that including the flow through the upstream piping geometry and including real gas effects will improve present results for these gases. However, the computational model had difficulty accurately characterizing the discharge coefficient for CO_2 ($U_r \approx 2\,\%$ of reading). Presently the mechanisms responsible for the discrepancy between numerical and experimental data are not clear, and further research is necessary.

The computational model was used to perform a parametric study investigating the effect of Re^*_{ideal}, γ, Pr, and wall thermal boundary condition on the discharge coefficient. For an adiabatic nozzle wall it was determined that Pr should have a negligible effect on C_d for most gases, and the assumption of $Pr = 1.0$ used in analytical studies causes little error in predicting C_d. The sensitivity analysis indicated that C_d was most sensitive to the wall thermal boundary condition at low Re^*_{ideal} for gas species with large γ. C_d for Ar decreased

by as much as 0.28 % at $Re^*_{ideal} = 3\,903$ indicating that wall heat transfer effects may need to be considered in analytical/numerical models seeking to perform beyond this level of accuracy.

Acknowledgements

Computational support was provided by the High Performance Systems and Service Division of the Information Technology Laboratory at NIST. In addition, enlightening discussions with Drs. Ronald W. Davis, Douglas A. Olson, and T. T. Yeh of NIST are gratefully acknowledged.

References

[1] John, J. E. A., "Gas Dynamics," *Allyn and Bacon, Inc.*, Newton, MA., 1984.

[2] Tang, S., "Discharge Coefficients for Critical Flow Nozzles and Their Dependence on Reynolds Numbers," Ph.D. Dissertation, Department of Mechanical Engineering, Princeton Univ., Princeton, NJ., 1969.

[3] Hall, I. M., "Transonic Flow in Two-dimensional and Axially-symmetric Nozzles," *Quart. J. Mech. and Applied Math.*, Vol. XV, Pt. 4, 1962, pp. 487–508.

[4] Geropp, D., "Laminare Grenzschichten In Ebenen Und Rotationssymmetrischen Laval-duesen," *Deutsche Luft- Und Raumfart, Forschungsbericht*, 1971, pp. 71–90.

[5] Tang, S. P., "Theoretical Dependence of the Discharge Coefficients of Axisymmetric Nozzles under Critical Flows," Technical Report PR-118-PU, Department of Mechanical Engineering, Princeton Univ., 1969.

[6] Ishibashi, M., and Takamoto, M., "Very Accurate Analytical Calculation of the Discharge Coefficients of Critical Venturi Nozzles with Laminar Boundary Layer," *Proceedings of the FLUCOME*, Hayama, Japan, Sept. 1–4, 1997.

[7] Nakao, S., Hirayama, T., and Takamoto, M., "Effects of Thermalphysical Properties of Gases on the Discharge Coefficients of the Sonic Venturi Nozzle," *Proceedings of the 1997 ASME Fluids Engineering Division Summer Meeting*, Vancouver, British Columbia, Canada, June 22–26, 1997.

[8] White, F.M., "Viscous Fluid Flow," *McGraw-Hill, Inc.*, New York, NY., 1991.

[9] Arnberg, B.T., Britton, C.L., and Seidl W. F., "Discharge Coefficient Correlations for Circular–Arc Venturi Flowmeters at Critical (Sonic) Flow," *ASME Journal of Fluids Engineering*, June, 1974.

[10] Buelow, P., Venkateswaran, S. and Merkle, C.L., "The Effect of Grid Aspect Ratio on Convergence," *AIAA Journal*, Vol.32, 1994, pp. 2401–2406.

[11] Feng, J., and Merkle, C.L., "Evaluation of Preconditioning Methods for Time Marching Systems," AIAA Paper 90–0016, AIAA 28th Aerospace Sciences Meeting, Reno, NV., 1990.

[12] Buelow, P.E.O., "Convergence Enhancement of Euler and Navier-Stokes Algorithms," Ph.D. Dissertation, Department of Mechanical Engineering, Pennsylvania State Univ., University Park, PA., 1995.

[13] ISO 9300: 1990 (E)., "Measurement of Gas Flow by Means of Critical Flow Venturi Nozzles," Geneva, Switz., 1990.

[14] Kruger, C.H., Walter G.V., "Introduction to Physical Gas Dynamics," *John Wiley & Sons, Inc.*, New York, NY., 1965.